Catalysis Today 144 (2009) 87–93

Contents lists available at ScienceDirect

Catalysis Today

journal homepage: www.elsevier.com/locate/cattod

Scaling-up of slurry reactors for the photocatalytic oxidation of cyanide with TiO_2 and silica-supported TiO_2 suspensions

Javier Marugán [a,*], Rafael van Grieken [a], Alberto E. Cassano [b,1], Orlando M. Alfano [b,1]

[a] Department of Chemical and Environmental Technology, ESCET, Universidad Rey Juan Carlos, C/Tulipán s/n, 28933 Móstoles (Madrid), Spain
[b] Instituto de Desarrollo Tecnológico para la Industria Química (INTEC), (Universidad Nacional del Litoral-CONICET), CCT Santa Fe. Paraje El Pozo. Colectora de la Ruta Nacional N 168, 3000 Santa Fe, Argentina

ARTICLE INFO

Article history:
Available online 1 February 2009

Keywords:
Photocatalysis
Large-scale reactor
Scaling-up
Cyanide
Titanium dioxide
Supported photocatalyst

ABSTRACT

A scaling-up methodology for the design of large-scale slurry reactors for the photocatalytic oxidation of cyanide is proposed. The only experimental information required to be determined at laboratory-scale is the intrinsic kinetics that describes the explicit dependence of the reaction rate with the local volumetric rate of photon absorption (LVRPA). Based on the kinetic model and the information about the geometry, irradiation source and the cyanide and catalyst concentrations as operation conditions, the performance of a larger scale reactor has been simulated following a predictive procedure with no adjustable parameters. The validation of the method has been carried out in a bench-scale reactor with ten times higher irradiated volume and a different geometry and irradiation source, in order to ensure that the conclusions about the applicability of the scaling-up model are independent of these parameters. The proposed scaling-up methodology and their correspondent procedures for the evaluation of the LVRPA distribution on the photoreactors has been successfully validated both with commercial TiO_2 and a silica-supported TiO_2 synthesized in our laboratory. The normalized root mean square error in the verification of the conversions predicted by the model for the larger scale reactor when compared with the experimental data are 7.7% and 6.2% for TiO_2 and TiO_2/SiO_2, respectively.

1. Introduction

The application of heterogeneous photocatalytic technologies for the oxidation of organic water pollutants has attracted increasing attention as the large number of scientific publications and reviews appeared in this field demonstrates [1–7]. However, up to date only relatively few developments have succeeded in the complete description of methodologies for the design of large-scale photocatalytic reactors, being most of the research efforts devoted to the investigation of the fundamentals and phenomenological aspects of the process.

In the case of the treatment of aqueous cyanide compounds, since the early work of Frank and Bard in 1977 [8], the photocatalytic oxidation has demonstrated a high efficiency in the removal of free cyanides [9–11] and also strong metal complexes [12–14] refractory to the traditional technologies for cyanide oxidation, such as alkaline chlorination or the use of ozone or hydrogen peroxide [15]. Most of the contributions devoted to the photocatalytic oxidation of cyanide are focused on the influence on the experimental reaction rate of variables such as catalyst loading, cyanide concentration, pH, presence of inorganic species, additional oxidants such as ozone or hydrogen peroxide, etc. [8–11]. There are been reported developments at pilot plant scale for the photocatalytic treatment of cyanides in effluents derived from integrated gasification combined cycle (IGCC) power plants [16] and electroplating factories [17], including their economic assessment, but without considering engineering models to verify the scaling-up predictions from laboratory data. Few kinetics studies have been performed, usually concluding that the dependence of the reaction rate with the concentration of cyanide followed the Langmuir–Hinshelwood kinetic equation [9–11]. These simple equations do not consider explicitly the local radiation absorption rate inside the photoreactor leading to equations that are only valid for the experimental setup in which the parameters have been estimated. Consequently, they become invalid for the design of photoreactors. It becomes necessary the determination of intrinsic kinetic models to describe the influence on the reaction rate of the local volumetric rate of photon absorption (LVRPA) in any position of the photoreactor volume [18–21].

* Corresponding author. Tel.: +34 91 664 7007; fax: +34 91 488 7068.
E-mail addresses: javier.marugan@urjc.es (J. Marugán), alfano@intec.unl.edu.ar (O.M. Alfano).
[1] Tel.: +54 342 451 1272/73; fax: +54 342 451 1087.

0920-5861/$ – see front matter © 2009 Elsevier B.V. All rights reserved.
doi:10.1016/j.cattod.2008.12.026

Nomenclature

C_{cat}	catalyst mass concentration (g cm$^{-3)}$
C_{CN^-}	cyanide molar concentration (mol cm^{-3})
$D^0_{CN^--Water}$	molecular diffusivity of cyanide ions in water (cm^2 s^{-1})
e^a	local volumetric rate of photon absorption, Einstein (cm^{-3} s^{-1})
L	nominal reactor length (cm)
Q	volumetric flow rate (cm^3 s^{-1})
r	radial cylindrical coordinate (cm)
R_{CN^-}	cyanide photooxidation reaction rate (mol cm^{-3} s^{-1})
S_g	TiO_2 specific surface area of the catalyst (cm^2 g^{-1})
t	time (s)
v_z	axial velocity (cm s^{-1})
V	volume (cm^3)
x	position vector in a 3D space (cm)
z	axial cylindrical coordinate (cm)

Greek symbols

α_1	kinetic parameter (cm s^{-1})
α_2	kinetic parameter (cm^2 s Einstein^{-1})
α_3	kinetic parameter (cm^3 mol^{-1})
χ	internal/external radius ratio
τ	residence time (s)

Subscripts

cat	relative to catalyst
CN^-	relative to cyanide
ext	relative to the external wall of the reactor
int	relative to the internal wall of the reactor
React	relative to the reactor
Tot	relative to the total recirculating system
Tank	relative to the reservoir tank
V_{React}	relative to the reactor volume

Superscripts

0	indicates initial condition
inlet	relative to the inlet stream

Special symbols

_	indicates a vectorial magnitude
$\langle\,\rangle$	indicates average value

Regarding the photocatalysts, attention has been paid to the development of supported materials in the form of fixed beds, fluidized beds or slurries [22], in order to avoid the cost of the catalyst recovery and the concerns about the potential toxicity of titanium dioxide nanoparticles [23]. Among them, silica-supported TiO_2 particulate materials appear to be a promising way to improve the recovery properties of the catalyst while maintaining an acceptable level of photoactivity [24].

Recent papers have reported different approaches for the development of scaling-up strategies for photocatalytic reactors [19,25–28]. However, none of them have been experimentally verified in slurry reactors using supported catalyst suspensions. In this study, a methodology for the scaling-up of slurry reactors for the photocatalytic oxidation of cyanide is proposed. The procedure is based on the experimental determination of the intrinsic kinetic parameters at laboratory-scale, in order to predict the performance of larger scale reactors without any adjustable parameter. The method has been validated in a bench-scale photoreactor with different geometry and irradiation source, both with commercial TiO_2 and silica-supported TiO_2.

2. Scaling-up methodology

The design of a large photocatalytic reactor requires the resolution of the mass balances for predicting the macroscopic conversion of the reactants. To evaluate the reaction rate under specific operations conditions, a kinetic model is considered, with parameters based on phenomenological or mechanistic basis. Simple equations such as the Langmuir–Hinshelwood kinetic model only takes into account the concentration of the reactants and products, whereas the effect of the catalyst concentration and the radiation flux is considered only implicitly in the kinetic constant. Consequently the derived kinetic expressions are only valid for the experimental setup in which have been developed and cannot be extrapolated to other reactor configurations.

The kinetic models required for the design of photocatalytic reactors must be independent on the experimental features of the reactor, and based on the detailed reaction mechanism of the process, including the radiation activated steps and therefore the rate of photon absorption. Thus, prior to the resolution of the mass balances, the radiation field in the irradiated volume of the photoreactor must be modelled and evaluated, due to the unavoidable radiation profiles always present in photocatalytic reactors that leads to non-uniform distribution of the local values of the radiation absorption rates and thus of the reaction rates. Fig. 1 summarizes the described methodology.

The validation of the proposed kinetic scheme and the estimation of the values of the kinetic parameters can be accomplished by an optimization algorithm that minimizes the error between the experimental results and the predicted values. Once the intrinsic kinetics of the process has been obtained exclusively with laboratory data, the design of the large-scale photoreactor can be accomplished. Obviously, the construction of the designed photoreactor and the comparison of its experimental conversions with the simulated values would allow the validation of the whole scaling-up procedure.

3. Experimental

3.1. Catalysts

Experiments and modelling have been carried out using a pure TiO_2 material commercially available (Aldrich, >99% anatase, 7.1 m^2 g^{-1} of specific surface area) and a home-made TiO_2/SiO_2 material with a nominal content of 40 wt.% of titania incorporated into a silica support (INEOS Silica ES70Y, 257 m^2 g^{-1} of specific surface area), synthesized through a sol–gel method. Characterization of this material shows that TiO_2 is homogeneously distributed over the silica porous network with an average crystallite size of 7.2 nm, leading to a titania surface area value of 19.3 m^2 g^{-1} [29]. More details about the physicochemical characterization and quantitative values of the optical properties of both catalysts suspensions can be found elsewhere [30].

3.2. Photoreactors

Fig. 2 represents the laboratory-scale photoreactor used for the determination of the intrinsic kinetic model. It is a 120 cm^3 cylindrical photoreactor, operating in a closed recirculating circuit driven by a centrifugal pump and with a stirred reservoir tank equipped with a device for withdrawal of samples. Illumination was

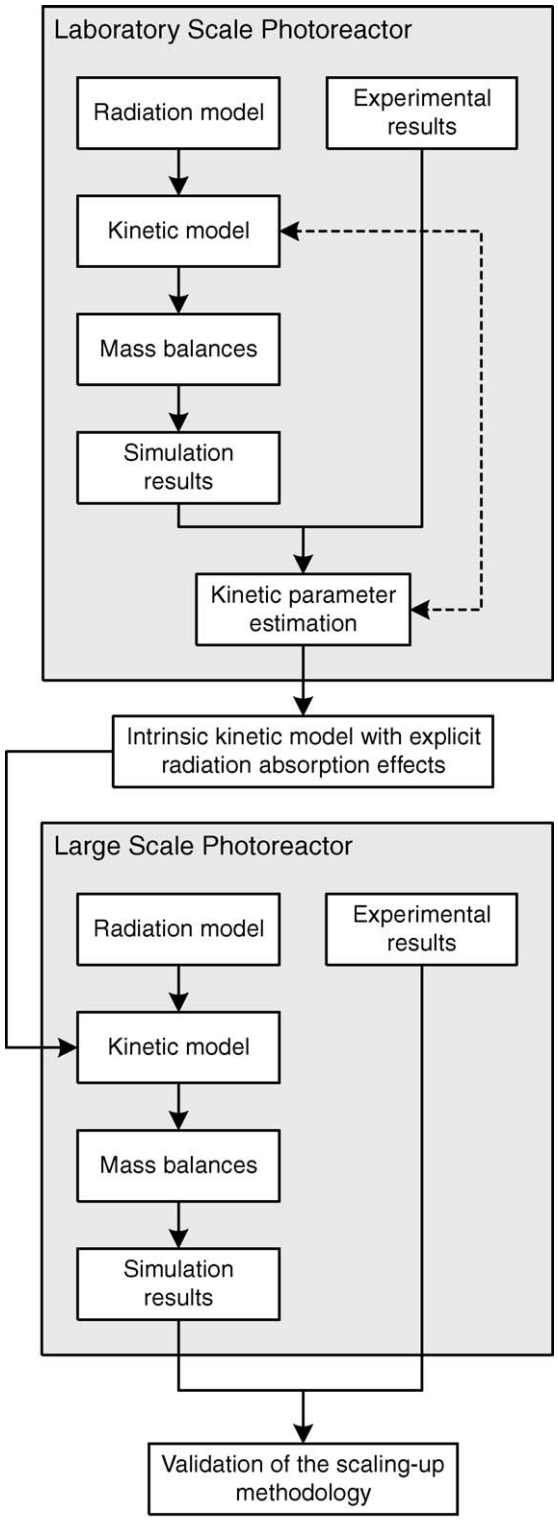

Fig. 1. Schematic flowchart of the scaling-up methodology for photoreactors.

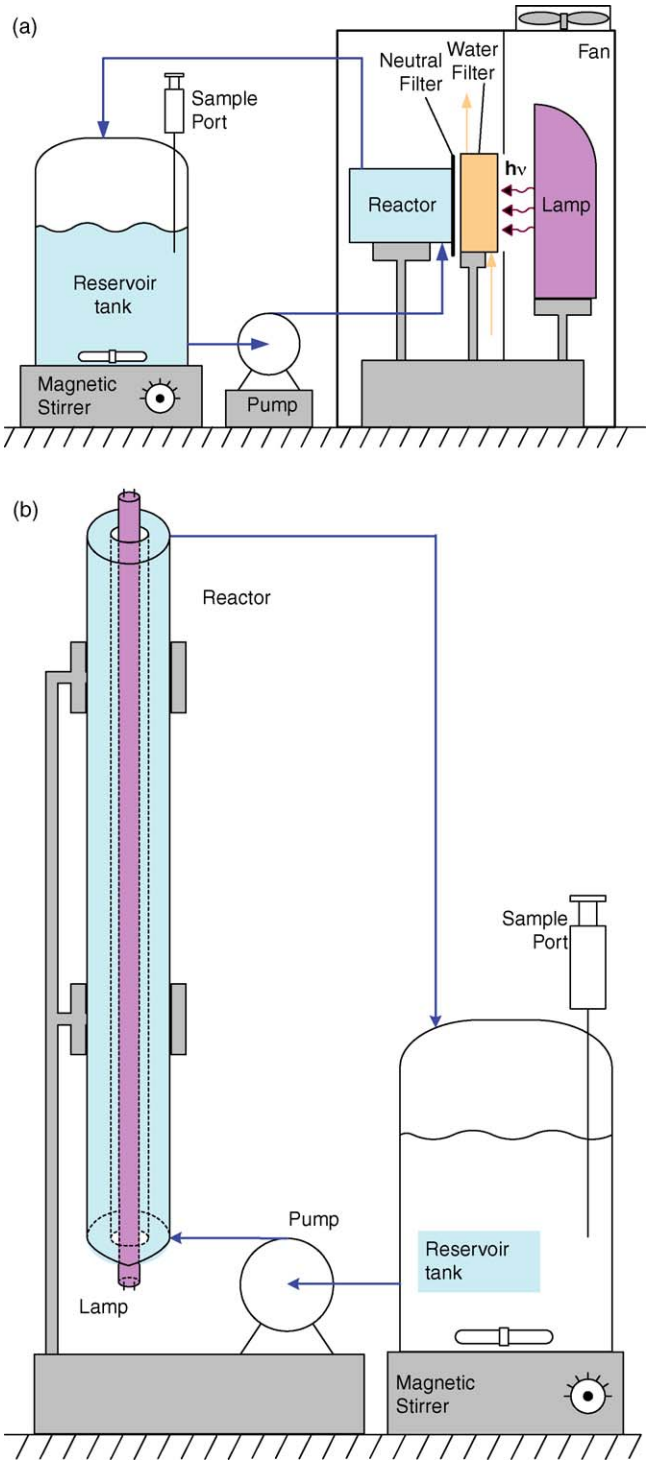

Fig. 2. Schematic representation of the laboratory-scale (a) and bench-scale (b) photoreactors (see text and Table 1 for details).

carried out using an Osram Ultramed 400W UV metal halide lamp that provides a high UV-A irradiation. The radiation flux entering the reactor was reduced to controlled values using neutral filters. More details about the reactor, filters, emission spectrum of the lamp and quantitative values of the radiation fluxes determined by ferrioxalate actinometry can be found elsewhere [31,32].

The bench-scale photoreactor setup for the validation of the scaling-up methodology (also represented in Fig. 2) is an annular photoreactor of 1250 cm^3 irradiated volume, operating in a closed recirculating circuit. Illumination was carried out using an Osram L 36W black light lamp with a maximum emission peak centred at 365 nm placed in the axis of the reactor. The UV-A incident photon flow determined by ferrioxalate actinometry was 1.8×10^{-5} Einstein s^{-1}. As it can be seen, this reactor has been designed for having a ten times higher irradiated volume than the laboratory-scale system, and it shows a totally different geometry and light

source, in order to assure that the validation of the scaling-up methodology is independent on these photoreactor characteristics.

Table 1 summarizes the main dimension and characteristics of the laboratory- and bench-scale reactors.

3.3. Reaction procedure

Experiments of cyanide photooxidation were carried out following the same procedure in both photoreactor setups. Reacting potassium cyanide (Panreac, reagent grade) solutions were prepared using deionized water (Milli-Q®, 18.2 MΩ cm) and adjusting the pH to 12 with sodium hydroxide (Scharlab, reagent grade). After adding the catalysts, the suspension was stirred and saturated with molecular oxygen by bubbling the gas for 30 min. In the meantime, the lamp was switched on to stabilize its emission power and spectrum.

Samples from the reservoir tank were taken every 10 min to follow the reaction evolution. After measuring temperature and pH to check that both parameters remained essentially constant, the catalyst was removed from the sample by filtering the suspension through 0.22 μm nylon membranes. Cyanide analysis was carried out using the pyridine–barbituric standard colorimetric method [33], taken the average concentration from four independent measurements.

4. Results and discussion

4.1. Determination of the intrinsic kinetics in the laboratory-scale photoreactor

As it is schematized in Fig. 1, simulation results of the photocatalytic cyanide oxidation can be computed from the cyanide mass balance in the reservoir tank. Assuming that: (i) the system is perfectly mixed; (ii) there are no mass transport limitations; (iii) the conversion per pass in the reactor is differential; and (iv) there are no parallel dark reactions, the mass balance can be expressed as follows:

$$\left.\frac{dC_{CN^-}(t)}{dt}\right|_{Tank} = -\frac{V_{React}}{V_{Tot}}\langle R_{CN^-}(\underline{x},t)\rangle_{V_{React}} \quad (1)$$

where V is the volume; Tank, React and Tot subscripts refer to the tank, reactor and total, respectively; t denotes reaction time; and $\langle R_{CN^-}(\underline{x},t)\rangle_{V_{React}}$ is the cyanide oxidation rate averaged over the reactor volume. This average reaction rate can be estimated by using a kinetic model and compared with that calculated from the experimental evolution of the cyanide concentration with time.

In a previous work [21] we have reported the development of an intrinsic kinetic model based on an accepted reaction mechanism and that takes into account explicitly the spatial variations of the LVRPA produced by the unavoidable radiation profiles existing in the photoreactor. The model takes the following expression:

$$R_{CN^-} = -S_g C_{cat}\frac{\alpha_1 C_{CN^-}}{1+\alpha_3 C_{CN^-}}\left[-1+\sqrt{1+\frac{\alpha_2}{S_g C_{cat}}e^a}\right] \quad (2)$$

where R_{CN-} is the cyanide disappearance rate, S_g the catalyst specific surface area, C_{cat} the catalyst mass concentration, C_{CN-} the cyanide molar concentration, e^a the LVRPA, and α_i (i = 1–3) are kinetic parameters.

According to Eq. (2), the evaluation of the reaction rate requires the estimation of the radiation field inside the photoreactor, in order to calculate the LVRPA. A detailed description of the numerical procedure for the resolution of the Radiative Transfer Equation (RTE) in the laboratory-scale photoreactor represented in Fig. 2, using a 2-dimensional 2-directional radiation model, can be found elsewhere [21].

Experiments in the laboratory-scale photoreactor shown in Fig. 2 were used for the estimation of the parameters of the kinetic model in the studied range of cyanide concentrations (0.185×10^{-6} to 3.85×10^{-6} mol cm^{-3}), incident radiation fluxes (0.255×10^{-6} to 2.89×10^{-6} Einstein cm^{-2} s^{-1}) and catalyst concentrations (0.32×10^{-4} to 5.0×10^{-4} g cm^{-3} for TiO_2 and 0.32×10^{-3} to 5.0×10^{-3} g cm^{-3} for TiO_2/SiO_2). These values were selected from literature [10,11] to cover the experimental region in which the reaction rate of cyanide photooxidation is clearly influenced by the studied variables.

Experimental results were compared with their correspondent simulation values to estimate the kinetic parameters α_1, α_2, and α_3 using a Marquardt–Levenberg non-linear regression algorithm. The values of the kinetic parameters thus obtained were:

$$\begin{aligned}\alpha_1 &= (6.34\pm0.11)\times10^{-6}\ \text{cm s}^{-1}\\ \alpha_2 &= (1.64\pm0.05)\times10^{11}\ \text{cm}^2\ \text{s Einstein}^{-1}\\ \alpha_3 &= 0\end{aligned} \quad (3)$$

for TiO_2 ($S_g = 7.1\times10^4$ cm^2 g^{-1}) and

$$\begin{aligned}\alpha_1 &= (9.94\pm0.14)\times10^{-7}\ \text{cm s}^{-1}\\ \alpha_2 &= (1.99\pm0.05)\times10^{11}\ \text{cm}^2\ \text{s Einstein}^{-1}\\ \alpha_3 &= (5.27\pm0.16)\times10^{5}\ \text{cm}^3\ \text{mol}^{-1}\end{aligned} \quad (4)$$

Table 1
Dimensions and characteristics of the laboratory- and bench-scale reactors.

Description	Laboratory-scale reactor	Bench-scale reactor
Main dimensions	Length = 6.0 cm Diameter = 5.0 cm	Length = 100.0 cm Inner diameter = 3.0 cm Outer diameter = 5.0 cm
Reactor volume	120 cm^3	1250 cm^3
Total system volume	1000 cm^3	4000 cm^3
Recirculation flow rate	100 cm^3 s^{-1}	65 cm^3 s^{-1}
Lamp type	Metal halide Osram Ultramed 400W/FDA R7S FS1	Black light fluorescent Osram L 36W/73 FLH1
Lamp position	External	Axial
Lamp dimensions	Length = 10.4 cm Diameter = 1.4 cm	Length = 120.0 cm[a] Diameter = 2.6 cm
Electrical input power	400 W	36 W
UV Emission range	320–400 nm	350–400 nm
Total radiation flow	0.5–5.7 × 10^{-5} Einstein s^{-1}	1.8 × 10^{-5} Einstein s^{-1}
Inlet radiation surface	19.6 cm^2	942.5 cm^2
Radiation flux	0.255–2.89 × 10^{-6} Einstein cm^{-2} s^{-1}	1.91 × 10^{-8} Einstein cm^{-2} s^{-1}

[a] Lamp positioned at z = 10 cm to minimize end effects.

for TiO_2/SiO_2 ($S_g = 19.3 \times 10^4\ cm^2\ g^{-1}$, corresponding only to the active semiconductor surface estimated using a previously reported method [29]).

The differences of the kinetic parameters corresponding to TiO_2 and TiO_2/SiO_2 are mainly derived from the differences in the optical properties of the materials. The absorption and scattering coefficients of the TiO_2/SiO_2 suspensions are much lower than those of TiO_2 suspensions [30]. In both cases the model reproduces the influence of the catalyst loading, the initial cyanide concentration, and the inlet radiation flux on the reaction rate, with errors below 5%, validating the kinetic model and the correspondent procedures for the evaluation of the LVRPA distribution and the estimation of the kinetic parameters. In the case of TiO_2, the removal of α_3 only produces a small increase in the error of the estimated parameters, whereas the plausibility of the model given by the *F*-test is substantially increased [21]. The values of the kinetic parameters in Eqs. (3) and (4) are independent of the irradiation form, as well as the reactor size and its geometrical configuration, providing the necessary information for scaling-up.

4.2. Validation of the scaling-up methodology in the bench-scale photoreactor

The designed bench-scale photoreactor posses an irradiated volume ten times higher than that of the laboratory-scale system. Moreover, it shows an annular geometry and a tubular black light fluorescent lamp, in contrast with the cylindrical geometry and the metal halide lamp used in the laboratory-scale photoreactor. It is important to remark that being rigorous the intrinsic kinetic model determined in the laboratory reactor (Eq. (2)) should only being applied to other reactor configurations using light sources with a similar spectral distribution of the emitted radiation. The reason is that the kinetic parameter α_2 defined during the derivation of the kinetic model [21] includes the value of the wavelength averaged primary quantum yield. In this case, although both lamp types are not exactly the same, the emission spectra are quite similar, with a maximum emission around 365 nm. In addition, the radiation emitted by the metal halide lamp at wavelengths greater than ~390 nm is not absorbed by the TiO_2 particles.

Consequently, we will assume that the values of the kinetic parameters shown in Eqs. (3) and (4), as a reasonable approximation, are valid for the bench-scale system.

As schematized in Fig. 1, simulation results of the photocatalytic cyanide oxidation can be computed from the cyanide mass balance equation. In contrast with the laboratory-system, in this case the photoreactor cannot be considered to be perfectly mixed, and consequently the differential form of the mass conservation equation must be used. Under the following assumptions: (i) steady state; (ii) negligible thermal effects; (iii) unidirectional axial flow; (iv) azimuthal symmetry; (v) negligible axial diffusion when compared to the convective flux in that direction; (vi) incompressible flow (constant ρ); and (vii) constant diffusion coefficient ($D^0_{CN^-\text{–Water}} = (1.25 \pm 0.05) \times 10^{-5}\ cm^2\ s^{-1}$ [34]), the mass balance can be expressed in cylindrical coordinates as follows:

$$v_z(r)\frac{\partial C_{CN^-}(z,r)}{\partial z} = D^0_{CN^-\text{–Water}}\left(\frac{1}{r}\frac{\partial}{\partial r}\left(r\frac{\partial C_{CN^-}(z,r)}{\partial r}\right)\right) + R_{CN^-}(z,r) \quad (5)$$

The boundary conditions for solving Eq. (5) are derived from the assumptions of: (i) the nominal reactor length, *L*, coincides with the effective length; and (ii) the reactor walls are non-permeable:

$$C_{CN^-}(z=0,r) = C_{CN^-}(t) \quad (6)$$

$$\frac{\partial C_{CN^-}(z,r_{int})}{\partial r} = \frac{\partial C_{CN^-}(z,r_{ext})}{\partial r} = 0 \quad (7)$$

The resolution of Eq. (5) requires the estimation of the velocity profiles in the annular space, $v_z(r)$, that under the assumptions of (i) laminar flow regime; (ii) Newtonian fluid; and (iii) negligible end effects, can be expressed as:

$$v_z(r) = 2\langle v_z\rangle \frac{1-(r/r_{ext})^2 + ((1-\chi^2)/(\ln(1/\chi)))\ln(r/r_{ext})}{(1-\chi^4)/(1-\chi^2) - (1-\chi^2)/(\ln(1/\chi))} \quad (8)$$

where $\chi = r_{int}/r_{ext}$ and $\langle v_z\rangle$ represents the average velocity, constant under incompressible flow conditions.

The solution of the cyanide differential mass balance in the photoreactor (Eq. (5)) also requires the description of the reaction rate $R_{CN^-}(z, r)$, given by the intrinsic kinetic model determined at laboratory-scale (Eq. (2)). For the evaluation of the reaction rate, the radiation field inside the photoreactor must be estimated. The resolution of the RTE in the bench-scale photoreactor represented in Fig. 2 has been carried out using a 2-dimensional 2-directional radiation model and a numerical procedure similar to that of the laboratory-scale photoreactor (detailed elsewhere [21]). The main difference was the determination of the inlet radiation boundary condition. Whereas in the laboratory-scale photoreactor a ground glass window allows the simplification to a diffuse irradiation inlet (equal intensities in all the directions), this hypothesis cannot be applied to the bench-scale reactor. In this case, the radiation emitted by the lamp is discretized into the different directions using a superficial diffuse emission model of the tubular lamp to take into account the geometry of the system [35]. Assuming that the optical properties of the suspension do not vary along the reaction, the LVRPA distribution evaluated on the photoreactor can be considered constant.

A Crank–Nicholson finite differences scheme has been used for the resolution of the mass balance Eq. (5). The solution leads to the distribution of the cyanide concentration on the reactor. Fig. 3 shows an example of the calculated cyanide concentration profiles. At constant value of *r*, a decrease of the concentration is observed along the *z*-axis of the reactor, in agreement with the increase in the residence time. In contrast, a strongly non-uniform distribution is observed along the radius of the reactor, with higher conversions near the reactor walls (due to the high values of the residence time produced by the velocity profiles) and with a substantially high conversion in the radiation entrance reactor

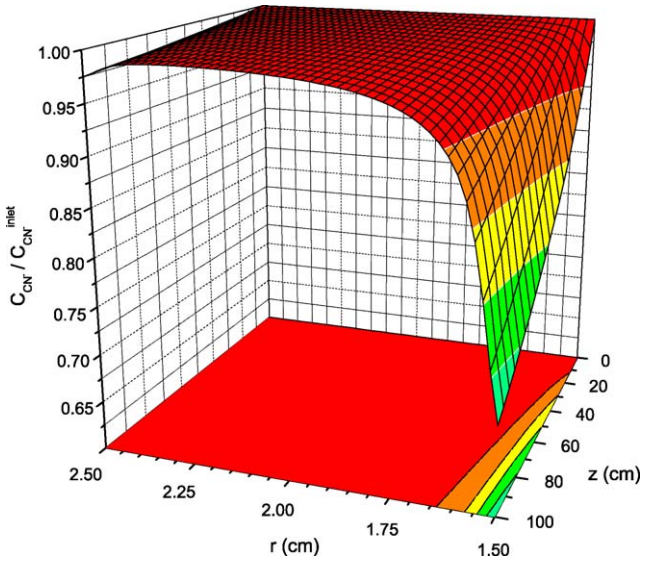

Fig. 3. Example of cyanide concentration profiles inside the photoreactor calculated from the resolution of the differential mass balance equation (inlet cyanide concentration: 30 mg L^{-1}; TiO_2 concentration: 0.5 g L^{-1}).

wall. However, it is worth mentioning that these concentration profiles have minor effect on the average cyanide conversion on the photoreactor, leading to values only 2% higher for hypothetical infinite diffusion coefficient.

Finally, the evolution of the cyanide concentration with time can be calculated through the resolution of the mass balance of the recirculating system. Assuming well mixing conditions on the reservoir tank, the mass balance takes the following expression:

$$\left.\frac{dC_{CN^-}(t)}{dt}\right|_{Tank} = \frac{1}{\tau_{Tank}}\left(C_{CN^-}^{inlet}(t) - C_{CN^-}(t)\right) \quad (9)$$

with the initial condition:

$$C_{CN^-}(t=0) = C_{CN^-}^{0} \quad (10)$$

Eq. (9) has been solved using a conventional Runge–Kutta numerical method in which the value of the inlet cyanide concentration is calculated from the outlet concentration of the reactor obtained through the resolution of the differential mass balance equation in the reactor (Eq. (5)).

Summarizing, the operation of the bench-scale reactor has been simulated following an absolutely predictive procedure that only requires information about the geometry of the system, the emission of the lamp and the operation conditions (catalysts concentration and initial cyanide concentration) and the determination at laboratory-scale of the intrinsic kinetic parameters.

Fig. 4 shows the comparison between the cyanide concentration profiles evolution with time obtained in the bench-scale photoreactor and the predicted values from the simulation model using TiO_2. In some cases, the predictions seem to overestimate the experimental conversion, although the discrepancies decrease as the catalyst concentration increases (Fig. 4a). Better predictions are also observed for the lower values of the initial concentrations of cyanide whereas the conversions for the highest values of C_{CN} are overestimated (Fig. 4b). In contrast, the simulation results using TiO_2/SiO_2 are in very good agreement with the experimental cyanide evolution determined for different values of the cyanide and catalyst concentrations (Fig. 5).

Whereas the experimental data for the predictions using TiO_2/SiO_2 are distributed at both sides of the prediction curves, in the case of the TiO_2 catalyst the predicted conversion results are usually overestimated. A possible explanation is that TiO_2 particles can suffer aggregation phenomena reducing the radiation absorption coefficients of the suspensions. Moreover, pure TiO_2 suspensions produce more fouling of the reactor glass inlet radiation window. Both factors can contribute to decrease the experimental conversion values. Finally, the differences already mentioned concerning the spectral distribution of the used lamps, should

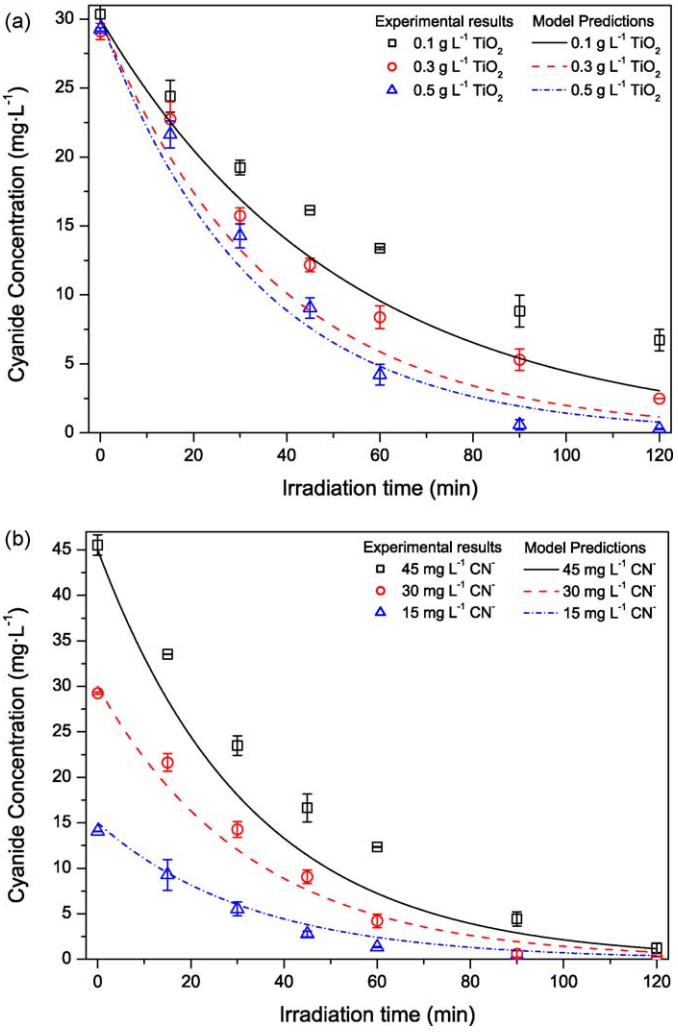

Fig. 4. Experimental results and model predictions of the operation of the bench-scale reactor using TiO_2: (a) effect of the catalyst concentration at fixed initial cyanide concentration of 30 mg L^{-1}; and (b) effect of the initial cyanide concentration at fixed catalyst concentration of 0.5 g L^{-1}.

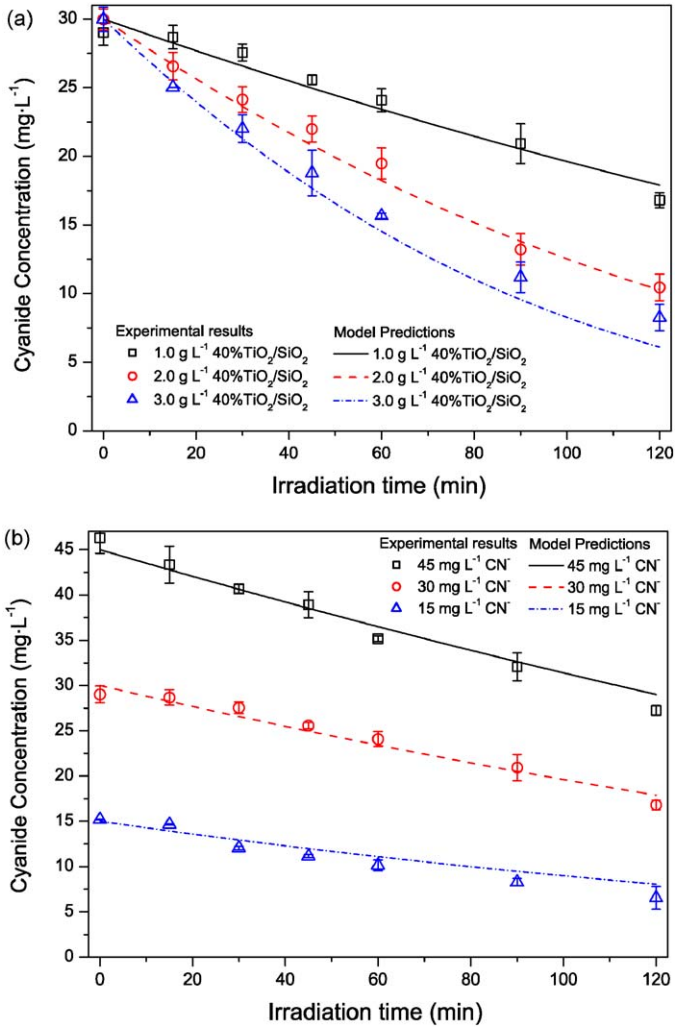

Fig. 5. Experimental results and model predictions of the operation of the bench-scale reactor with TiO_2/SiO_2: (a) effect of the catalyst concentration at fixed initial cyanide concentration of 30 mg L^{-1}; and (b) effect of the initial cyanide concentration at fixed catalyst concentration of 1.0 g L^{-1}.

certainly produce a decrease in the efficiency of the second reactor as compared with the results in the laboratory reactor. In fact, the observed deviations are in the correct direction. In any case, the values for the normalized root mean square errors are 7.7% for TiO_2 and 6.2% for TiO_2/SiO_2. These values can be considered satisfactory, specially taking into account that the simulation has been performed without making use of any adjustable parameter.

5. Conclusions

The proposed method for the scaling-up of slurry reactors for the photocatalytic oxidation of cyanide has been successfully validated both with commercial TiO_2 and a silica-supported TiO_2 synthesized in our laboratory. The procedure is based on the determination of the intrinsic kinetics of the reaction at laboratory-scale to describe the explicit dependence of the reaction rate with the radiation profiles existing in the photoreactor. Based on this information, the model of a larger scale reactor has predicted with good accuracy its experimental performance. Therefore, this scaling-up methodology can be used in a predictive way for the simulation and optimization of any other reactor configuration for the photocatalytic oxidation of cyanide as well as scaling-up and large photoreactor design purposes.

Acknowledgements

The authors gratefully acknowledge the financial support of the Ministerio de Educación y Ciencia of Spain through the program Consolider-Ingenio 2010 (project CSD2006-00044 TRAGUA) and the international action PCI2006-A7-0526, Comunidad de Madrid through the program REMTAVARES S-0505/AMB/0395 and from the Universidad Nacional del Litoral, Agencia Nacional de Promoción Científica y Tecnológica, and Consejo Nacional de Investigaciones Científicas y Técnicas of Argentina. Thanks also to Ing. Rosa Massanet for her valuable help with some of the experiments.

References

[1] D.F. Ollis, H. Al-Ekabi (Eds.), Photocatalytic Purification and Treatment of Water and Air, Elsevier, Amsterdam, 1993.
[2] D. Blake, Bibliography of Work on the Photocatalytic Removal of Hazardous Compounds from Water and Air, NREL, Golden, CO, 1994(1st update: October 1994; 2nd update: October 1996; 3rd update: January 1999; 4th update: October 2001).
[3] M.R. Hoffmann, S.T. Martin, W. Choi, D.W. Bahnemann, Chem. Rev. 95 (1995) 69.
[4] J.M. Herrmann, Catal. Today 53 (1999) 115.
[5] D.S. Bhatkhande, V.G. Pangarkar, A.A. Beenackers, J. Chem. Technol. Biotechnol. 77 (2001) 102.
[6] A. Mills, S.K. Lee, in: S. Parsons (Ed.), Advanced Oxidation Processes for Water and Wastewater Treatment, IWA Publishing, London, UK, 2004.
[7] A.G. Agrios, P. Pichat, J. Appl. Electrochem. 35 (2005) 655.
[8] S.N. Frank, A.J. Bard, J. Am. Chem. Soc. 99 (1977) 303.
[9] J. Peral, J. Muñoz, X. Domènech, J. Photochem. Photobiol. A: Chem. 55 (1990) 251.
[10] V. Augugliaro, V. Loddo, G. Marcì, L. Palmisano, M.J. López, J. Catal. 166 (1997) 272.
[11] K. Chiang, R. Amal, T. Tran, J. Mol. Catal. A: Chem. 193 (2003) 285.
[12] V. Augugliaro, E. García López, V. Loddo, M.J. López-Muñoz, G. Marcì, L. Palmisano, M. Schiavello, Fresenius Environ. Bull. 8 (1999) 350.
[13] R. van Grieken, J. Aguado, M.J. López-Muñoz, J. Marugán, Gold Bull. 38 (4) (2005) 180.
[14] R. van Grieken, J. Aguado, M.J. López-Muñoz, J. Marugán, Appl. Catal. B: Environ. 55 (2005) 201.
[15] C.A. Young, T.S. Jordan, Proc. 10th Annual Conference on Hazardous Waste Research, Kansas State University, Manhattan, Kansas, (1995), pp. 104–129.
[16] V. Augugliaro, J.C. Conesa, E. García López, V. Loddo, M.J. López Muñoz, G. Marcì, L. Palmisano, M. Schiavello, J. Soria, Chimica e L'industria 83 (2001) 34.
[17] A. Vidal, P. Trincado, M. Jerez, M. Vincent, J. Blanco, S. Malato, P. Fernández, Ingeniería Química Enero (2001) 161.
[18] O.M. Alfano, M.I. Cabrera, A.E. Cassano, J. Catal. 172 (1997) 370.
[19] M. Rodríguez, S. Malato, C. Pulgarin, S. Contreras, D. Curcó, J. Giménez, S. Esplugas, Solar Energy 79 (2005) 360.
[20] I. Salvado-Estivill, D.M. Hargreaves, G. Li Puma, Environ. Sci. Technol. 41 (2007) 2028.
[21] J. Marugán, R. van Grieken, A.E. Cassano and O.M. Alfano, Appl. Catal. B: Environ. (2008) doi:10.1016/j.apcatb.2008.06.026.
[22] R.L. Pozzo, M.A. Baltanás, A.E. Cassano, Catal. Today 39 (1997) 219.
[23] J.R. Gurr, A.S.S. Wang, C.H. Chen, K.Y. Jan, Toxicology 213 (2005) 66.
[24] J. Aguado, R. van Grieken, M.J. López-Muñoz, J. Marugán, Appl. Catal. A: Gen. 312 (2006) 202.
[25] H. de Lasa, B. Serrano, M. Salaices, Photocatalytic Reaction Engineering, Springer, Berlin, Germany, 2005.
[26] M.L. Satuf, R.J. Brandi, A.E. Cassano, O.M. Alfano, Catal. Today 129 (2007) 110.
[27] G. Camera-Roda, F. Santarelli, Ind. Eng. Chem. Res. 46 (2007) 7637.
[28] G. Li Puma, B. Toepfer, A. Gora, Catal. Today 124 (2007) 124.
[29] J. Marugán, M.J. López-Muñoz, J. Aguado, R. van Grieken, Catal. Today 124 (2007) 103.
[30] J. Marugán, R. van Grieken, O.M. Alfano, A.E. Cassano, AIChE J. 52 (2006) 2832.
[31] J. Marugán, R. van Grieken, A.E. Cassano, O.M. Alfano, Int. J. Chem. Reactor Eng. 5 (2007) A89.
[32] J. Marugán, R. van Grieken, A.E. Cassano, O.M. Alfano, Catal. Today 129 (2007) 143.
[33] L.S. Clescerl, A.E. Greenberg, A.D. Eaton (Eds.), Standard Methods for the Examination of Water and Wastewater, United Book Press Inc., Baltimore, 1998.
[34] X. Sun, Y.C. Guan, K.N. Han, Metall. Mater. Trans. B 27 (1996) 355.
[35] A.E. Cassano, C.A. Martin, R.J. Brandi, O.M. Alfano, Ind. Eng. Chem. Res. 34 (1995) 2155.